CSCE Annual Conference

Growing with youth – Croître avec les jeunes

Laval (Greater Montreal)

June 12 - 15, 2019

HIGH STRENGTH CONCRETE COLUMNS REINFORCED WITH BFRP BARS AND TIES UNDER ECCENTRIC LOADS

Ashraf Salah-Eldin[1], Hamdy M. Mohamed[1], and Brahim Benmokrane[1]

[1]Department of Civil Engineering, University of Sherbrooke, Sherbrooke, Quebec, Canada

Abstract: This paper presents the results of a research program investigating the use of newly developed sand-coated basalt-FRP (BFRP) bars and ties in axial–flexural members made with high-strength concrete (HSC). Four full-scale concrete columns 400 *400 mm in cross section and 2,000 mm in height were constructed and tested. The test variables were eccentricity-to-depth ratio and reinforcement type (BFRP and steel bars and ties). The test results indicate that the specimens reinforced with BFRP bars and ties under different levels of eccentricity behaved similarly to their steel-reinforced counterparts. An analytical study was conducted to predict the axial–flexural capacity. The findings of this investigation can be considered as a fundamental step toward developing code provisions for using BFRP bars and ties as internal reinforcement in different structures such as bridge pier and pile applications.

1 INTRODUCTION

Bond Experimental Work Heavily loaded structures, such as bridges and high-rise buildings, require additional attention from designers regarding durability issues, choosing the right materials, and reducing maintenance costs. For bridges, using high-strength concrete offers many advantages that could help reduce construction costs and increase structure service life. It allows for smaller cross sections due to its higher compressive strength, reduced creep and shrinkage, lower deflection due to a higher modulus of elasticity, and increased durability as well as enhanced physical- and chemical-deterioration resistance (Smadi et al., 1987; Mokhtarzadeh and French, 2000). HSC has been increasingly used in precast bridge elements, thereby facilitating and shortening bridge construction (Mokhtarzadeh and French,2000). Despite these advantages, HSC is still subject to steel-corrosion problems, which reduces service life and durability. In order to overcome this problem, fiber-reinforced-polymer (FRP) reinforcement is being used extensively as a replacement for steel reinforcement in US and Canadian bridges. It is also considered an economical, less-disruptive solution compared to retrofitting structural elements after degradation has occurred.

Valuable research has been carried out in recent years on the behavior of glass-FRP (GFRP) bars in compression members. Afifi et al. 2014; De Luca et al. 2010; Tobbi et al. 2014; and Hadhood et al. 2017a tested square and circular concrete columns reinforced with GFRP and demonstrated the viability of using GFRP in axially loaded RC members for bridge pile and pier applications. The contribution of the GFRP bars in compression was reported to range from 3% to 10% of the total load-carrying capacity of the RC columns compared to 12% to 16% for steel reinforcement. Hadhood et al. (2017b) tested full-scale columns made with HSC and reinforced with GFRP bars and spirals tested under concentric and eccentric loading.

Their results indicate that increasing the GFRP-reinforcement ratio enhanced the stiffness of the concrete columns. Guérin et al. (2018) tested and reported experimental data for full-scale square concrete columns reinforced with GFRP bars and ties. The columns were tested under four different values of eccentricities. Their performance was compared to four control specimens reinforced with steel bars and ties. The test results indicated that the steel- and GFRP-reinforced concrete columns behaved similarly and that GFRP bars and ties could be used effectively in compression members.

Recently, basalt-FRP (BFRP) has emerged as a promising alternative to conventional FRPs in reinforcing concrete structures (Elgabbas et al. 2015 and 2016). BFRP bars show advantageous mechanical and chemical characteristics as well as a higher performance–cost ratio compared to other FRPs. For instance, BFRP has higher strength and modulus at a similar cost; greater chemical stability than E-glass FRP; a wider range of working temperatures; and much lower cost than carbon FRP (CFRP) (Sim et al. 2005). It has also shown to perform better in an acidic environment (Wei et al. 2010) and provide five times the strength and approximately one-third the density of commonly used low-carbon steel bars (Sim et al. 2005). Because of these characteristics, BFRP bars were chosen for the HSC columns in this study.

2 Materials

The specimens were all cast with ready-mixed concrete with a water-to-cement ratio of 0.32. The cement was Type GUb-8SF, which was premixed with silica fume and water reducer, as shown in Table 2. The silica-fume percentage was 9.4% by mass. The slump was around 80 mm (before adding the superplasticizer). The concrete strength was determined in accordance with ASTM C39/C39M by testing 150 × 300 mm cylinders that were cured under conditions similar to that of the specimens. The concrete cylinders had an average strength of 71.2 MPa on the day of testing.

2.1.1 BFRB bars

BFRP bars (No. 6; 19 mm diameter) were used as longitudinal reinforcement on the tension and compression sides and No. 4 (13 mm diameter) BFRP ties were used as transverse reinforcement, see Fig. 1. Crossties were used at the center of the cross section with tail lengths equal to 12 d_b (d_b is the tie diameter). The BFRP bars were manufactured from continuous basalt fibers impregnated in vinyl-ester resin using the pultrusion process with a fiber content of 81% (by weight). The ultimate tensile strength, f_{fu}, and the modulus of elasticity, E_f, of the longitudinal BFRP bars (No. 6) and the straight portion of the bent BFRP bars (No. 4) were determined according to ASTM D7205.

2.1.2 Steel bars

The steel reinforcement consisted of grade 60 steel bars used in the control specimens. Deformed M20 steel bars were used as the longitudinal reinforcement and M10 for the ties. Table 1 provides the properties and dimensions of both the steel and BFRP bars.

Figure 1: BFRP reinforcing bars

Table 1: Properties of the BFRP and Steel reinforcement

RFT type	Bar Size	d_b, mm	A_f [a], mm^2	A_{im} [b], mm^2	E_f, GPa	f_{fu}, MPa	ε_{fu}, %
BFRP	No.4	13	129	86.8 ± 3.6	51.4±0.18	1414 [d] ±11	2.75±0.2
	No.6	20	285	309 ± 4.5	63.7±0.81	1646±40	2.50±0.1
Steel	10M	11.3	100	---	200	f_y [c] = 460 ± 10	ε_y [c] = 0.2
	20M	19.5	300	---	200	f_y [c] = 460 ± 15	ε_y [c] = 0.2

[a] Nominal cross-sectional area.
[b] Immersed cross-sectional area.
[c] f_y and ε_y are the yield strength and strain of the steel bars, respectively.
[d] Tensile strength of straight bar.
Note: properties calculated based on the nominal cross-sectional area

2.2 Test specimens

Full-scale columns were made with HSC: four were reinforced with BFRP bars and ties and four with steel reinforcement as control specimens. All the columns measured 400 * 400 * 2,000 mm. The concrete cover was kept constant at 35 mm for all specimens. Each group of columns with the same type of reinforcement was tested under four different eccentricity-to-depth ratios (0.2, and 0.6*h* where *h* is the depth of the square section). The eccentricities were selected to test the columns under large and small eccentricity where: *e/h* = 0.2: small eccentricity (compressive stress behavior is dominant); *e/h* = 0.6: large eccentricity (tensile-stress behavior is the dominant transition zone: flexural behavior. Each specimen was labelled so as to indicate the reinforcement type and applied eccentricity. The letters B and S identify specimens reinforced with BFRP or steel, respectively. The numbers 80, 240 after the *e* symbol represents the applied eccentricity in millimeters, check Table 2. The reference steel-reinforced concrete columns had the minimum amount of longitudinal reinforcement and the minimum tie cross-sectional area at maximum spacing (16d_b, where d_b is the bar diameter). The same longitudinal reinforcement ratio (1% A_g, where A_g is the gross area of the column's cross section) was used for the BFRP-reinforced concrete specimens with three BFRP bars (No. 6) on each side of the column. As specified by ACI 318-14's maximum tie spacing (16d_b), as per Sections 10.7.6.1.2 and 25.7.2.1, was reduced to 8d_b for the BFRP reinforced columns to account for the difference in moduli of elasticity between BFRP and steel reinforcement (Guérin et al. 2018; De Luca et al. 2009). Figure 2 shows the reinforcement details for both column series.

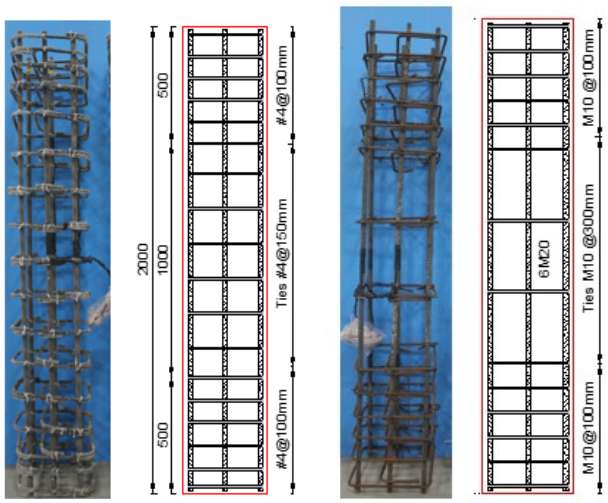

Figure 2: Reinforcement details.

Table 2: Test matrix and reinforcement details

Series	Col. ID	e (mm)	e/h (%)	Reinforcement	
				longitudinal	Transverse
Basalt	Be80	80	20	6 No. 6	No.4 @ 150 mm
	Be240	24	60	6 No. 6	No.4 @ 150 mm
Steel	Se80	80	20	6 20M	No.3 @ 300 mm
	Se240	240	60	6 20M	No.3 @ 300 mm

2.3 Instrumentation and test setup

The compressive and tensile strains induced in the reinforcement bars during testing were measured with electrical resistance strain gauges mounted at the middle of the reinforcement bars. The tensile and compressive strains were measured at the mid-height of the columns. A total of four electrical strain gauges were used to monitor the strains along the BFRP rebars. The horizontal deflection was measured with linear variable displacement transducers (LVDTs) fixed at three different points along the column: mid-height and the top and bottom quarter of the column. Moreover, two strain gauges were mounted on the surface of the concrete columns to monitor the compressive concrete strain at the surface. The loading, deflection, and strains in the concrete and reinforcement were recorded with an automatic data-acquisition system connected to a computer. Figure 3 shows the overview of the test setup. The test setup was designed and fabricated in the University of Sherbrooke's structural laboratory. Rigid steel caps were designed and fabricated to provide proper confinement and prevent premature failure of the end zones. The top and bottom surfaces of the columns were filled with high-strength cement grout to maintain full contact between the column sides and the end caps. The load was applied at the determined eccentricity using roller bearings attached to the steel end caps. The columns were observed visually during testing for cracks and the corresponding loads were recorded.

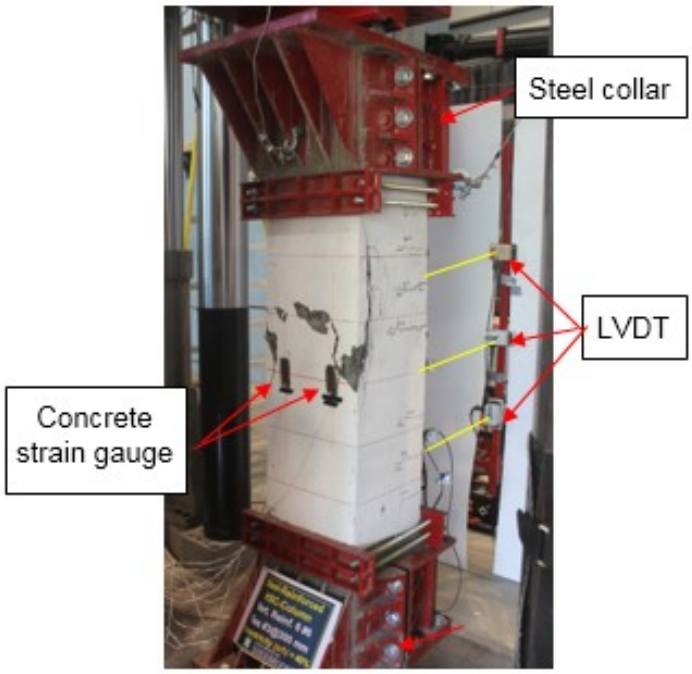

Figure 3: Test Setup.

3 Experimental Test Results

3.1 Columns tested with small eccentricity (0.2h)

The basalt- and steel-reinforced columns had similar behavior and failure modes when tested under an eccentric load of 0.2*h*. Table 3 shows the summary of the test results. The concrete cover on the compression side was visually free of cracks until 90% of the peak load. The tensile cracking patterns initiated at column mid-height where the maximum moment is expected. More cracks appeared as the loading continued, increasing until reaching the failure load. The failure was identified by concrete-cover spalling on the compression side, as shown in Fig. 4. Columns Be80 and Se80 sustained maximum loads of 4,965 kN, and 5,137 kN, respectively. Figs. 5 (a), and (b) provide the load versus axial and lateral deflections, respectively. At peak load, Se80 had smaller axial- and lateral-deflection values (11.74 mm and 3.79 mm) compared to Be80, which reached axial and lateral displacements of 9.20 and 5.13 mm, respectively. At peak load, the recorded average strain for the compression bars was -1,930 με and -2,680 με for Be80 and Se80, respectively, as shown in Fig. 7. The strain values for the steel bars on the compression side indicated that the steel bars had reached yielding strains before reaching peak load. When the yielding strain was reached, the steel bars buckled outwards, which facilitated spalling of the concrete cover. This spalling led to axial-strength loss and a sudden increase in lateral deformation. The strength loss after peak load was 44% and 49% for Be80 and Se80, respectively. It should be noted that, due to the reinforcement yielding, the steel-reinforced columns had larger concrete-crushing areas and permanent deformation even after load removal. In contrast, the BFRP-reinforced columns retained smaller axial and lateral deformation even after concrete-cover spalling. Moreover, wider cracks were observed in the steel-reinforced column in the post-peak phase.

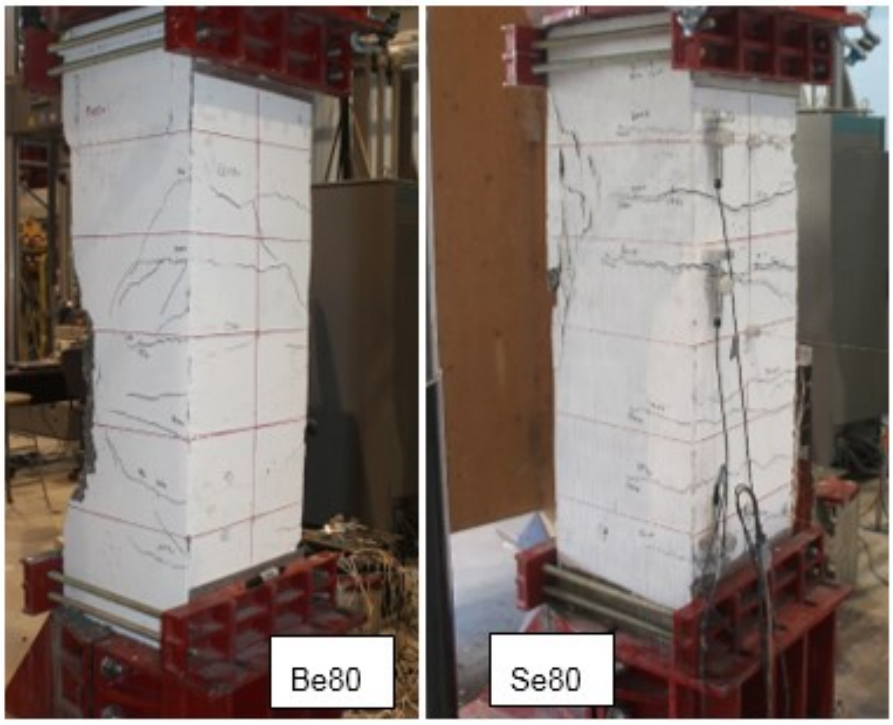

Figure 4: Crack pattern at failure of the tested columns at e = 0.2 h.

Table 3: Summary of test results.

Series	Column ID	*e/h*	P_{peak} (kN.m)	e (mm)	Δ (mm)	M_I (kN.m)	M_{II} (kN.m)	M_{tot} (kN.m)	$P_{bar,peak}$ (kN)
B	Be80	0.2	4965	80	5.13	397	25	423	210
	Be240	0.6	1309	240	22.7	314	30	344	105
S	Se80	0.2	5137	80	3.8	411	19	411	335
	Se240	0.6	1338	240	15.21	321	20	321	315

Notes: *e* is eccentricity; *h* is column depth; P_{peak} is peak axial load; M_{tot} is the total moment due to the applied eccentricity and the secondary moment due to the deflection; and $P_{bar\ peak}$ is the bar contribution at peak load.

3.2 Columns tested with large eccentricity (0.6h)

With both types of reinforcement, applying the axial load at such a high level of eccentricity resulted in greater flexural response of the columns. The cracking stresses were reached at a very early stage of loading. Subsequently, flexural tensile cracks started to appear and widened along the length of the columns, which experienced more axial and lateral deformation as the axial load increased. On the other hand, higher tensile and compressive strains were reached in the tensile and compressive BFRP bars. In the case of the columns loaded with high eccentricity—Be240 and Se240—the flexural stresses dominated the failure process of the columns' critical section. The steel-reinforced column had a bilinear load–axial gradient up to a maximum axial resistance of 1,338 kN. Its first crack occurred at a load of 300 kN (26% of peak load), then tensile cracks started spreading along the length of the column. At a load of 1,280 kN, the tensile bars reached yield strain and, simultaneously, the cracks grew wider and deeper. Based on the load versus mid-height deflection shown in Fig. 5 (b), the specimen exhibited much lower lateral stiffness, which suddenly increased the rate of lateral deflection. At this point, the column is classified unsafe due to excessive deflection and wide cracks. That occurred with Se240. The peak resistance was reached when the concrete strain recorded was 3,100 με. At this level of eccentricity, the steel bars buckled outwards which contributed to spalling of the concrete cover, as shown in Fig. 6.

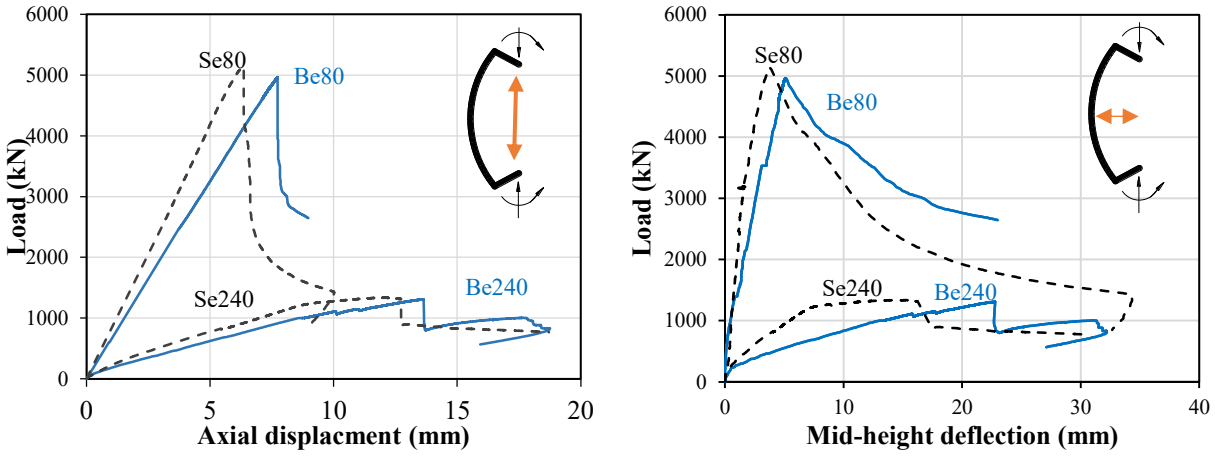

Figure 5: Axial Load versus (a) axial displacement; and (b) mid-height deflection.

Column Be240 exhibited a failure process similar to that of its counterpart Se240. For column Be240, the cracking started at the middle top and bottom of the testing zone at a load of 280 kN (22% of peak load). As the load increased, the flexural cracks propagated deeper into the column, and more cracks started to

develop along the tensile surface. At such a high *e/h* ratio, the axial load had little effect on reducing the cracks width; the flexural moment controlled the column's failure process. A slight dip in load was noticed before reaching the maximum load, followed by the column resisting more axial load. The column Be240 failed at a load of 1,309 kN. It was noticed that the steel-reinforced counterpart, Se240, had sudden spike in the rate of increase in lateral deflection at a load level of 1,230 kN and lateral deflection of 9.0 mm. This is attributed to the yielding of the tensile bars. Conversely, Be240 did not experience any reduction in lateral stiffness before reaching the peak load. The failure of the column Be240 was marked by spalling of the concrete cover at a concrete strain of 2,770 με. At failure, the column Be240 reached an axial deflection of 13.6 mm and lateral deflection of 22.8 mm. The recorded strain for the compressive bars was 1,910 με (7% of ultimate strain) and 9,300 με (36% of ultimate strain) for the tensile bars. In the post-failure phase, the column, Be240, showed increase in strength, reaching a second peak at a load of 1,000 kN. The maximum recorded strains for the basalt bars were 5,570 με (22% of ultimate strain) for the compressive bars and 10,930 με (42% of ultimate strain) for the tensile bars. The test stopped when the column evidenced no sign of further increase in strength. After load removal, Be240 recovered most of the deflection as the basalt bars did not reach the ultimate rupture or crushing strains. Small residual deformation was still observed due to crushing of the concrete during the failure process.

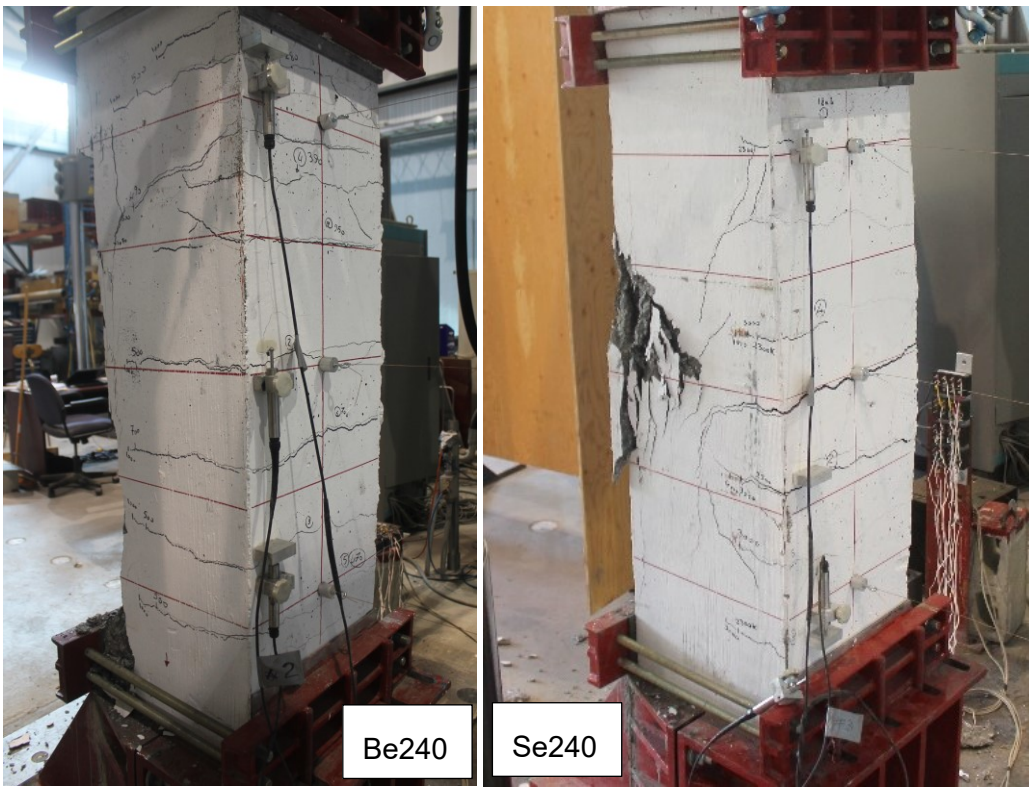

Figure 6: Crack pattern at failure of the tested columns at e = 0.6h.

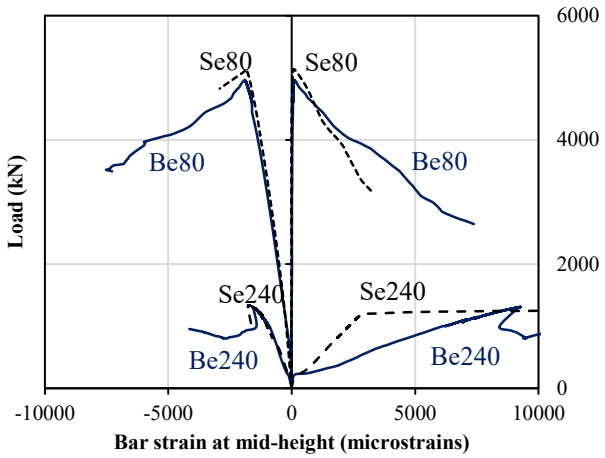

Figure 7: Measured bar strain at mid-height.

4 Effect of test parameters

4.1 Effect of reinforcement type

The bar strains were monitored with electric strain gauges mounted at column mid-height on the compressive and tensile bars, and at the quarter height for the tensile bars only (see Fig. 7). Given the bar strain, the bar's contribution was calculated by multiplying the strain by the bar's Young's modulus. Table 4 shows that the average load carried by the longitudinal BFRP reinforcement was 4.2%, and 8% for Be80, and Be240, respectively. The values for the steel-reinforced counterparts were 6.5%, and 23% for Se80, Se240, respectively. The difference in the bar load contribution was expected, since the Young's modulus of the steel bars is more than three times that of the basalt bars. This also accounts for the difference in the axial resistance between the BFRP- and steel-reinforced columns.

Furthermore, based on the experimental data in our study, the BFRP-reinforced columns exhibited behavior similar to the steel-reinforced columns in terms of crack propagation, axial and lateral deflection, and levels of axial strength. For the post-peak phase, the basalt bars exhibited lower strength losses due to their linear elastic nature. The BFRP bars effectively resisted the tensile forces on the tension side of the columns after concrete crushing and failure of the BFRP bars on the compression side. The basalt ties exhibited no rupturing in either the pre-peak or post-peak phases for the eccentricities tested. Thus, BFRP reinforcement can be used as a valid replacement for steel reinforcement in corrosive environments because of their non-corrodible nature and high tensile strength.

5 Conclusions

Based on the experimental test results and analysis presented in this paper, the following conclusions can be drawn:

1. Using BFRP reinforcement in HSC columns yielded axial resistance close to that of steel-reinforced columns at eccentricity-to-depth ratios of 0.2h and 0.6h. The difference in strength did not exceed 3%, this is attributed to the yielding of the steel bars in the steel reinforced columns at these eccentricities.

2. Both types of reinforcement were able to achieve stable and ductile behavior in the pre-peak phase. The BFRP bars developed up to 4,000 με compressive strain, confirming that the BFRP bars were effective in resisting compression until concrete cover crushing.

3. Using tie spacing of $8d_b$ (half of that specified in ACI 318-14 to account for the difference in moduli of elasticity between the steel and BFRP reinforcement) for the BFRP-reinforced HSC columns provided sufficient lateral support to prevent crushing of the BFRP bars and the concrete core. Also, the concrete core was able to continue withstanding the applied load in the post-peak phase, and the BFRP bars developed maximum compressive strains and tensile strains of 6,700 με 10,900 με.

6 Acknowledgments

This research was conducted with funding from the Tier-1 Canada Research Chair in Advanced Composite Materials for Civil Structures, the Natural Sciences and Engineering Research Council of Canada (NSERC), the NSERC Industrial Research Chair in FRP Reinforcement for Concrete Infrastructure, the Fonds de recherche du Québec en nature et technologies (FRQ-NT), and the Quebec Ministry of Transportation. The authors would like to thank Pultrall Inc. (Quebec, Canada) and Mafic USA (North Carolina, USA) for donation of BFRP reinforcement, and the technical staff of the Canadian Foundation for Innovation (CFI) structural & materials lab in the Department of Civil Engineering at the University of Sherbrooke.

7 References

ACI (American Concrete Institute). (2014). “Building code requirements for structural concrete.” ACI 318-14M, Farmington Hills, MI.

ACI (American Concrete Institute). (2015). “Guide for the design and construction of concrete reinforced with FRP bars.” ACI 440.1R-15, Farmington Hills, MI.

ASTM D7205/D7205M-06(11), 2011. “Standard Test Method for Tensile Properties of Fiber Reinforced Polymer Matrix Composite Bars,” ASTM International, West Conshohocken, PA.

Afifi, M. Z., Mohamed, H. M., and Benmokrane, B. (2014). “Axial Capacity of Circular Concrete Columns Reinforced with GFRP Bars and Spirals.” *Journal of Composites for Construction*, 18(1), 1–10.

De Luca, Matta, F., and Nanni, A. (2009). “Behavior of Full-Scale Glass Fiber-Reinforced Polymer Reinforced Concrete Columns under Axial Load.” *ACI Structural Journal*, 107(5), 589-596.

Elgabbas, F., Ahmed, E. A., and Benmokrane, B. (2015). “Physical and mechanical characteristics of new basalt-FRP bars for reinforcing concrete structures.” *Construction and Building Materials*, Elsevier Ltd, 95, 623–635.

Elgabbas, F., Ahmed, E. A., and Benmokrane, B. (2016). “Experimental Testing of Concrete Bridge-Deck Slabs Reinforced with Basalt-FRP Reinforcing Bars under Concentrated Loads.” *Journal of Bridge Engineering*, 21(7), 04016029.

Guérin, M., Mohamed, H. M., Benmokrane, B., Nanni, A., and Shield, C. K. (2018a). “Eccentric Behavior of Full-Scale Reinforced Concrete Columns with Glass Fiber-Reinforced Polymer Bars and Ties.” *ACI Structural Journal*, 115(2), 489–500.

Hadhood, A., Mohamed, H. M., and Benmokrane, B. (2017a). “Strength of circular HSC columns reinforced internally with carbon-fiber-reinforced polymer bars under axial and eccentric loads.” *Construction and Building Materials*, Elsevier Ltd, 141, 366–378.

Hadhood, A., Mohamed, H. M., and Benmokrane, B. (2017b). “Failure envelope of circular concrete columns reinforced with glass fiber-reinforced polymer bars and spirals.” *ACI Structural Journal*, 114(6), 1417–1428.

Mokhtarzadeh, A., and French, C. (2000). “Mechanical Properties of High- Strength Concrete with Consideration for Precast Applications,” *ACI Materials Journal*, 97(2), 136-147

Sim, K., Park, C., and Moon, D. Y. (2005). “Characteristics of basalt fiber as a strengthening material for concrete structures.” *Composites Part B: Engineering*, Elsevier Ltd, 36(6–7), 504–512

Smadi, Mohammed M., Slate, Floyd O. and Nilson, Arthur H. (1987), “Shrinkage and creep of high, medium, and low strength concretes, including overloads.” *ACI Materials Journal*, 84(3), 224-234.

Tobbi, H., Farghaly, A. S., and Benmokrane, B. (2014). “Behavior of concentrically loaded fiber-reinforced polymer reinforced concrete columns with varying reinforcement types and ratios.” *ACI Structural Journal*, 111(2), 375–385.

Wei, B., Cao, H., and Song, S. (2010). “Environmental resistance and mechanical performance of basalt and glass fibers.” J. Mater. Sci. Eng. Part A, 527(18–19), 4708–4715.